[TO APPEAR IN *LASER PHYSICS*]

Quantum interference and its potential applications in a spectral hole-burning solid

Byoung S. Ham,[1,] Philip R. Hemmer,[2] Myung K. Kim,[3] and Selim M. Shahriar[1]

[1]Research Laboratory of Electronics, Massachusetts Institute of Technology, Cambridge, Massachusetts 02139

[2]Air Force Research Laboratory, Hanscom Air Force Base, Massachusetts 01731

[3]Department of Physics, University of South Florida, Tampa, Florida 33620

Abstract

We have reviewed observations of electromagnetically induced transparency (EIT) in solids and its potential applications such as enhanced four-wave mixing, Raman excited optical memory, and rf-coupled optical gain.

Introduction

In a three-level system, a resonant laser field can experience absorption reduction when a second resonant "coupling" field is applied, due to destructive quantum interference between two absorption pathways. Manifestations of this effect include coherent population trapping[1,2] (CPT) and in an optically thick medium (especially for pulsed excitation) electromagnetically induced transparency (EIT).[3] Since the first observations of absorption reduction in sodium vapors[1] and beams[2], there have been many studies of CPT and EIT for potential applications such as quantum noise quenching,[4] lasers without inversion (LWI),[5] efficient up-conversion lasers,[6] pulse propagation dynamics,[7] turbulence aberration correction,[8] spectroscopy,[9] precision magnetometry,[10] and optical memories.[11] EIT has attracted much recent interest because it allows the use of optically dense, resonant media for nonlinear optical applications. So far all the experiments mentioned above have been done with atomic beams or vapors. The diffusion of atoms in gas media, however, is a major problem and limits applications, especially when one is working with optical images. To overcome this disadvantage, spectral hole-burning solids are a natural choice because of the absence of diffusion and the similarity of their optical properties to atomic vapors. In addition, these materials exhibit permanent optical pumping (storage capability). Although oscillator strengths in spectral hole-burning solids are much weaker ($f \sim 10^{-7}$) than most atomic vapors, the absorption lines are narrow (1-10 GHz) and inhomogeneously broadened, optical decay times are slow (10-100 μs), and energy sub-level splittings are resolvable. Because of the absence of diffusion, the study of EIT in such solids is important for applications such as image processing, real-time holography,[12] optical memory,[13] optical switches,[14] turbulence diagnostics,[15] coherence spectroscopy,[16] and quantum computing.[17] The first observations of EIT in solids were in ruby where low lying Zeeman states were coupled with strong microwave fields (16.3 GHz) using V- and cascade-schemes.[18] Efficient EIT in an optically solid material was first observed in a rare-earth crystal, Pr^{3+} doped Y_2SiO_5 (Pr:YSO), using a Λ-scheme.

In the present paper, we review observations of EIT,[19,20] enhanced four-wave mixing generation,[20] Raman optical data storage,[13] and rf-coupled optical gain in Pr:YSO.[21] We also discuss the potential applications of EIT in spectral hole-burning materials to LWI and optical memory.

Figure 1 shows an energy level diagram of Pr:YSO. Our system consists of 0.05 at. % Pr^{3+} doped YSO in which Pr^{3+} ions act like an inhomogeneously broadened six-level atomic system. For this work, the relevant optical transition is $^3H_4 \leftrightarrow {}^1D_2$, which has a resonant frequency of 606 nm (at site 1). The optical population decay time T_1 and phase decay time T_2 are 164 μs and 111 μs, respectively at 1.4 K.[22] The optical inhomogeneous width is ~ 4 GHz. We observed that the optical homogeneous width increases exponentially as temperature increases from 4 K to 6 K in Pr:YSO, while the spin homogeneous width is almost constant.[13] The ground ($^3H_4$) and excited ($^1D_2$) state each has three doubly degenerate hyperfine states.[22] The splittings between the hyperfine states of the ground level are 10.2 MHz ($\pm 1/2 \leftrightarrow \pm 3/2$), 17.3 MHz ($\pm 3/2 \leftrightarrow \pm 5/2$), and 27.5 MHz ($\pm 1/2 \leftrightarrow \pm 5/2$).[23] The ground state population decay time T_1 is ~100 s,[22] and spin transverse decay time T_2 for the 10.2 MHz transition is 500 μs at 6 K.[13] For the 10.2 MHz transition, we measured an inhomogeneous linewidth of 29 kHz by use of an rf-optical double resonance technique.[24] Due to the relatively slow population decay time among the hyperfine sublevels of the ground level, optical spectral hole-burning persists unless the populations are redistributed among the three hyperfine levels by an optical or microwave field. The measured absorption coefficient for the optical transition in Pr:YSO is α=10 cm^{-1}, when spectral hole-burning is neglected.

The laser fields at ω_1 and ω_2 in Fig. 1 act as pump beams, which create a sublevel coherence ρ_{12} through CPT or EIT. Here, it should be noted that the pump Rabi frequency Ω does not necessarily have to be strong to reach near maximal coherence, because the Raman coherence amplitude depends on the pulse area Θ: $\Theta = \int_0^t \Omega(t')dt'$.[25] However, in an optically thick medium a strong Rabi frequency is necessary and in fact desirable for achieving strong four-wave mixing signals with EIT. To satisfy the

two-photon resonance condition, the difference frequency of the pump beams ω_1 and ω_2 should match a ground state hyperfine splitting, and for maximum effect at low optical powers each optical frequency should be resonant to its respective transition. The laser field ω_P acts as a probe (read) beam, which scatters off of the two-photon coherence created by the pump beams. For non-collinear pump beams, a coherence grating is formed and a four-wave mixing signal ω_D is generated, satisfying the phase matching condition $\mathbf{k_D}=\mathbf{k_1}-\mathbf{k_2}+\mathbf{k_P}$. The repump field ω_R is essential to prevent all population from ending up in the ±5/2 ground sublevels (see Figure 1) because of the 100 sec population lifetime. Varying the strength of this repump controls the effective optical density of the crystal in much the same way that changing the temperature of an atomic vapor affects its optical density. The repump field ω_R can also provide spectral selectivity in the otherwise broadband inhomogeneous system (~4 GHz inhomogeneous width) since only the repumped atoms will interact with the EIT fields. The amount of spectral selectivity provided by the repump depends on the laser jitter in our experiments. Here it should be emphasized that the precise level assignment in Figure 1 would not be possible without spectral hole-burning and a repump. Otherwise, each laser field would simultaneously drive all the transition shown in Figure 1 for a subset of Pr-ions somewhere in the inhomogeneous line. With persistent optical pumping (spectral hole-burning) and the repump, we insure that only Pr-ions having all three ground states excited by optical transitions contribute to the signal. We have verified this spectral selectivity by scanning the repump beam frequency over a range spanning all three excited states. When the repump beam is resonant with a transition to one of the excited states, the probe beam is absorbed; otherwise the crystal looks transparent.

Experimental setup

Figure 2 shows a schematic of an experimental setup for observing EIT and four-wave mixing in Pr:YSO. We use a frequency stabilized Coherent ring dye laser pumped by a Spectra Physics argon ion laser. The laser is continuous wave, and measured linewidth is 1-2 MHz when stabilized. We use acousto-

optic modulators (AO) driven by frequency synthesizers to make four different coherent laser beams having correlated frequency jitter, as shown. To avoid coherent interaction between the repump and the two-photon transition, the repump transition is chosen as shown in Fig. 1. All four laser beams are focused into the sample by a 40 cm focal length lens. The beam diameters (1/e in intensity) are ~ 150 μm in the crystal. The angle between the two pump beams is ~ 70 mrad. The hole-burning crystal Pr:YSO is inside the helium cryostat. At temperatures over 10 K, no spectral hole-burning was observed. The optical B-axis of the sample is along the laser propagation direction.

4. Results and discussion

4. 1. Efficient EIT

Figures 3(a) - 3(d) show the absorption spectra of the probe field (ω_1) in Pr:YSO at 2 K, when the coupling field (ω_2) intensities are (a) 9 W/cm^2, (b) 28 W/cm^2, (c) 90 W/cm^2, and (d) 280 W/cm^2.[19] The intensities of the probe (ω_P) and repump (ω_R) fields are held fixed at 9 W/cm^2 and 16 W/cm^2, respectively. For this EIT experiment, however, ω_P is blocked. The laser frequency is tuned near the center of 4 GHz inhomogeneously broadened absorption profile of Pr:YSO. The full width at half maximum (FWHM) of the observed absorption spectrum in Figure 3 is about 1.2 MHz, which is similar to the laser jitter. In all cases, the absorption curve disappears when the repump field is blocked, as expected. Due to EIT, the transmission of the probe field at line center increases from near 0 % to (a) 3 %, (b) 14 %, (c) 36 %, and (d) 65 %, where the higher transmission corresponds to the higher coupling field intensity. It should be noted that the actual absorption linewidth should be slightly wider than that measured in Fig. 3, because the AO varies the probe beam angle along with its frequency, so that for large detunings, there is laser beam walk-off and repumping no longer occurs. Experimentally, we find that the beam walk-off becomes important for the probe detunings greater than ±1 MHz. The noise on wings of the absorption spectra come from the combined effects of laser jitter and the spectral hole burning processes.

To better study the coupling field intensity dependence of EIT, we measured the widths of the transparency windows in Figs. 3. The measured FWHMs are (b) 23 kHz, (c) 30 kHz, and (d) 63 kHz. All the EIT linewidths are much narrower than the laser jitter and comparable to the spin inhomogeneous linewidth (29 kHz) of the 10.2 MHz transition. This insensitivity to correlated laser jitter is the signature of the two-photon transitions responsible for EIT. The line narrowing of the EIT window in Figure 3(b) is attributed to the high optical density.[26]

In Fig. 4 we observed asymmetric EIT, when the coupling field ω_2 is off resonance. This is accomplished by detuning the repump frequency by (a) 300 kHz and (b) 600 kHz from the resonance, which is the same as detuning the coupling field by the same amount in the opposite direction. Here, we should note that negative detuning means blue probe detuning and vice versa. As seen in Fig. 4, the effective absorption line-center is blue-shifted by an amount equal to the repump field detuning, and there is asymmetric EIT on the two-photon resonance, which is in agreement with off-resonant CPT or EIT measurements made in atomic beams (V-scheme)[27] and vapors (cascade scheme).[28] For this data, the intensity of the coupling field is 90 W/cm^2.

We also studied EIT in Pr:YSO at higher temperatures. We observed near 100 % transmission of the probe field at line center, when the coupling field intensity is 900 W/cm^2 at 6 K. The intensities of the probe and repump fields were at 14 W/cm^2 and 11 W/cm^2, respectively. We also found that the EIT induced transparency decreases as temperature increases. This should be explained by noting that as temperature increases the dephasing rate of the optical transitions increase because of phonon interactions. This higher dephasing rate leads to smaller ground state coherence at a fixed laser intensity and weaker EIT. In Pr:YSO, the optical dephasing rate rapidly increases as temperature increases beyond 4 K. We have observed efficient EIT up to 8 K with the maximum coupling laser intensity of 900 W/cm^2.

4. 2. Enhanced four-wave mixing

Figures 5 show enhanced four-wave mixing (FWM) owing to EIT.[20] The laser intensities of ω_1, ω_2, ω_P, and ω_R are 60, 40, 20, and 60 mW/cm^2. Fig. 5(a) shows the transparency window for ω_2 without the read beam ω_P, and the absorption change is 15%. The spectral width of the reduced absorption is 60 kHz. For the four-wave mixing experiment, we unblocked the read beam ω_P, which is blue-detuned by 100 kHz from the resonance frequency of ω_2 (see Fig. 1). Even though this detuning is smaller than the laser jitter, ω_P and ω_2 are never degenerate, because the fields are generated with AOs from a single laser (see Fig. 2). The alignments of laser beams ω_1, ω_2, and ω_P satisfy Bragg condition for the generation of ω_D at the position indicated in the inset in Fig. 2, which shows the spatial positions of the four laser beams on a screen after passing through the crystal. Figure 5(b) shows the intensity of the diffracted signal ω_D as a function of the detuning of ω_2. The diffracted signal ω_D is enhanced greatly as the beam ω_2 is tuned through two-photon resonance. The FWHM of the four-wave mixing signal is 40 kHz which approximately matches the width of the EIT transparency window. The diffraction efficiency, i.e., intensity ratio of ω_D to ω_P is ~ 1 %. Again, sub-laser-jitter linewidth is the evidence of EIT. Therefore the enhancement of nonlinear generation of the FWM signal is due to the ground state coherence produced by EIT.

4. 3. Raman excited spin echoes

In this section, we discuss how EIT can be used for fast optical excitation of a large-amplitude spin coherence using relatively low intensity lasers. This technique relies on the shelving of atomic population in the excited state via a resonant Raman π-pulse. We also show that efficient echo generation can be accomplished by applying a Raman 2π-pulse. Although this technique has not been previously demonstrated using optical excitation, the π–2π echo model was predicted in quantum-beat,[29] and it was experimentally performed in microwave regime.[30] The echo efficiency in this microwave experiment was poor because it was based on a Raman-like system in which only one of the two electron-spin transitions was allowed.

To illustrate this technique in more detail, consider a three-level Λ-type system interacting with two resonant Raman fields (see Fig. 6(a)), described in terms of dark ($|-\rangle$) and bright ($|+\rangle$) states (see Fig. 1(b)). These are defined as:

$$|-\rangle = \left[\Omega_2 |1\rangle - \Omega_1 |2\rangle\right] / \Omega, \qquad \text{(1-a)}$$

$$|+\rangle = \left[\Omega_1 |1\rangle + \Omega_2 |2\rangle\right] / \Omega, \qquad \text{(1-b)}$$

where $\Omega = \sqrt{\Omega_1^2 + \Omega_2^2}$ and Ω_1, Ω_2 are the Rabi frequencies coupling states $|1\rangle$, $|2\rangle$ to state $|3\rangle$, respectively. In the coherent state basis (Fig. 6(b)), only the bright state $|+\rangle$ is coupled to the excited state $|3\rangle$ so that the system behaves like a two-level atom with an additional uncoupled state into which population can be trapped. The ground state spin coherence r_{12} can be expressed in this basis as,

$$\mathrm{Re}(r_{12}) = [\, r_{++} - r_{--}] / 2, \qquad \text{(2)}$$

where r_{++} and r_{--} are the ensemble averaged populations in the $|+\rangle$ and $|-\rangle$ states, respectively.

In the limit of long excited state lifetime (or large Rabi frequency), the dynamics are simply explained by Rabi flopping. In this case, the ground state spin coherence has sinusoidal time dependence as shown by the solid curve in Fig. 6(c). Here, equal Rabi frequencies have been assumed. As expected, maximum coherence (of -1/4) occurs for an optical pulse area of π, which corresponds to zero bright state population $r_{++} = 0$. In the opposite limit of fast excited state lifetime (or small Rabi frequency), the spin coherence gradually increases to its maximum value (of -1/2) as the $|+\rangle$ state is emptied via optical pumping or CPT. This is shown by the dotted curve in Fig. 6(c). An intermediate case is plotted as the dashed curve which shows how the spin coherence evolves when the optical transition has a long excited state population decay time, but short coherence decay time. Here, the spin coherence initially evolves sinusoidally, but the oscillations rapidly damp out as the optical coherence dephases.

To understand how resonant Raman excitation can initiate rephasing (echoes), consider an atom left in only the $|-\rangle$ and $|3\rangle$ states by the first pulse. Due to inhomogeneous broadening on the spin transition, the $|-\rangle$ state will acquire a $|+\rangle$ state contribution with time *t* according to:

$$\left|y_{ground}(t)\right\rangle = \left[\cos(d \cdot t/2)|-\rangle + i\sin(d \cdot t/2)|+\rangle\right] \tag{3}$$

where *d* is the detuning from two-photon (Raman) resonance for an atom away from the center of the inhomogeneously broadened transition. If at time t = *T* a second resonant Raman pulse is applied, the $|+\rangle$ and $|3\rangle$ state contributions are exchanged by Rabi flopping. After an optical 2π-pulse, the $|+\rangle$ state amplitude is returned to its original value, except for a π phase shift. This gives a new ground state contribution,

$$\left|y'_{ground}(T)\right\rangle = \left[\cos(d \cdot T/2)|-\rangle - i\sin(d \cdot T/2)|+\rangle\right] \tag{4}$$

It is easy to show that this state evolves to a pure $|-\rangle$ state at time t = 2*T* that is independent of *d*, thereby producing an efficient spin echo. Finally, the excited state $|3\rangle$ will also experience dephasing between pulses, especially in the presence of optical inhomogeneous broadening. However, this will not be rephased by the optical 2π-pulse. Thus, even if the second pulse area is not exactly 2π, the excited state contribution will not adversely affect the spin echo.

To generate pulses, we added rf switches driven by pulse generators (SRS DG 535) to control rf powers to the AOs. Typical pulse sequences begin with a 3 ms repump pulse (ω_R), followed immediately by the first resonant Raman pulse (ω_1 & ω_2). The second resonant Raman pulse is applied with a variable delay of time T from the first pulse. The first pulse width is 8 μs, and the second pulse width is 16 μs. The probe pulse (ω_P) has a width of 10 μs, and its delay time is scanned from just before the end of the repump pulse (-10 μs delay) to beyond the echo location in steps of 1 μs. The repetition rate of the entire pulse sequence is 50 Hz. To average out laser jitter effects, thirty diffracted signals are captured by a Boxcar averager (SRS 250) using a gate width of 5 μs positioned on top of the probe pulse.

Figure 7(a) illustrates the typical experimental resonant Raman pulse sequence. As mentioned above, each resonant Raman pulse is composed of both ω_1 and ω_2, and the second pulse is twice as wide as the first pulse. Fig. 7(b) shows the Raman excited spin free induction decay (FID) and echo signals, as detected by monitoring the diffracted beam ω_D.[25] The signal is strong enough to be detected by a photodiode instead of a photomultiplier as is normally used for optical echoes. The pulse separation T is chosen to be 1/10 of the spin T_2, and close to the optical population lifetime T_1. As shown in Fig. 7(b), the spin echo efficiency is 21 % of FID signal in intensity. We found that the echo signals are not very sensitive to the width of either Raman pulse in the range of 5 μs - 20 μs. From this, we suspect that the laser jitter is greater than the optical Rabi frequency (see Fig. 4 of Ref. 25). The noise in the FID and echo signals come from both laser intensity and frequency jitter. The broader than expected FID signal width is attributed primarily to convolution with the relatively wide (10 μs) the probe pulse width.

In the limit of crystal length *l* longer than the laser beam overlap length, the four-wave mixing signal intensity (I_D) is attenuated by a factor of $\exp(\alpha l)$:

$$I_D(l) \propto [\mathrm{Re}(\rho_{12})]^2 \cdot I_P(0) \cdot \exp(-\alpha l), \qquad (5)$$

where α is an absorption coefficient, ρ_{12} is Raman coherence, and $I_P(0)$ is the probe intensity at z=0. Measurements in atomic and molecular vapors[31,32] predict that the four-wave mixing signal in relation (5) will be proportional to the product of the pump intensities ω_1 and ω_2 until saturated is reached. This is because the Raman coherence ρ_{12} is proportional to the product of pump Rabi frequencies (for weak pump beams). In addition, the Raman coherence ρ_{12} is expected to be position dependent due to the large linear absorption. However, this is suppressed in our experiment by using enough pump energy to saturate the transitions. Therefore, the Raman pump pulse excited spin coherence ρ_{12} is nearly position invariant and the diffracted signal only depends on optical density αl as, $\exp(-\alpha l)$. Here it has been assumed that the read beam is strongly absorbed when not overlapped with the pump fields, as is the case in the experiment. Note that the when laser beam overlap length is comparable to crystal length, relation (5) can be modified

by replacing *l* with *l'*, the length in the crystal over which there is no overlap. From this discussion, it is clear that using a thin sample is better for efficient, large-angle wavemixing.

Figure 7(c) shows numerical simulations of the Raman coherence intensity ($\mathrm{Re}(\rho_{12})$) as a function of time.[25] This calculation assumes a closed three-level system with equal initial ground state populations. The excited state population decay rate Γ was chosen to be 10 kHz which is close to the actual lifetime at 5 K, and the optical coherence decay rate γ was chosen to be 100 kHz which is close to the measured decoherence rate due to the laser jitter. For simplicity, the spin decay rates were set to zero. The spin inhomogeneous width was assumed to be 30 kHz with a Gaussian lineshape. The optical Rabi frequency was chosen to be similar to the laser jitter (100 kHz). The first pulse width was adjusted to give a π–pulse and the second pulse width was set for a 2π–pulse. The calculated echo efficiency is ~ 18 % in intensity, which is comparable to the experimental value in Fig. 7(b).

We did more theoretical analyses of Raman excited spin echoes and found that in the case of a large optical homogeneous dephasing rate γ, the echo amplitude does not depend strongly on the Raman pulse area. This case is analogous to the CPT limit in that the excited atoms have dephased, but not yet decayed to the ground states. The fact that the echo efficiency is still close to 20 % for $\gamma >> \Omega$ implies that even low-power lasers should give easily observable echoes, and therefore be adequate for many applications.

4. 4. Optical data storage

Figure 8 shows the storage of two bits of time-domain optical data by frequency-selective stimulated spin echoes excited by EIT.[13] Each input pulse is composed of resonant Raman beams (ω_1 & ω_2). The first two input pulses (d and d') are data bits. The second and third input pulses are write (w) and read (r) pulses, respectively. The pulse width of the repump beam is 1 ms (not shown), and immediately precedes the data pulse d. The pulse widths of the data bits (d and d') are 7 μs and 2 μs,

respectively, separated by 100 μs. The widths of the write and read pulses (w and r) are 7μs and 5μs, respectively, separated by 1.1 ms which is about twice the spin T_2 (500 μs). The time delay between data pulse d' and the write pulse w is 300 μs, which is chosen to be longer than the optical T_2 (111 μs) but shorter than the spin T_2. The probe (ω_P) pulse width is 5μs, and the diffracted signals (30 samples) are averaged by a Boxcar averager. When the input pulses are present, the diffracted signals are off-scale on the chart recorder. As seen in Fig. 8, 'two-pulse' echoes are observed soon after the write pulse w. The echo signal e is bigger than e' because the data d has a wider area than d'. The stimulated echoes are retrieved by the read pulse r and appear at $t_3 + t_2$ and $t_3 + t_2 - t_1$. Their intensities are comparable with those of the 'two-pulse' echoes. As is well known, for stimulated echoes, the theoretical storage time is limited by a spin population decay time T_1, which is ~ 100 s in this material. The maximum storage density under optimal experimental conditions is determined by the ratio of optical inhomogeneous width to spin homogeneous width, which is $\sim 10^7$ in Pr:YSO. Unlike optical echoes, this ideal storage capacity should be possible at higher temperatures due to the smaller temperature sensitivity spin homogenous width.

4. 5. Rf-coupled optical gain

Figure 9(a) shows optical gain in a cascade scheme when the 10.2 MHz ground state spin transition (see Figure 1) is coupled by resonant rf fields.[21] For this data, ω_1 and ω_P are blocked (see Figure 1). Due to spectral hole burning, the laser fields deplete all Pr-ions from state $|2\rangle$ to state $|1\rangle$ before the rf pulse comes. When the rf pulse arrives, the optical field ω_2 starts to be absorbed by the repopulated Pr-ions. The rf Rabi frequency can be easily measured by measuring rf nutation frequency. The measured rf Rabi frequency Ω_{rf} is 28 kHz. As seen in Fig. 9(a), at the end of the first 2π rf Rabi oscillation, there is an optical gain. This gain mostly comes from the population inversion ($\rho_{33} > \rho_{22}$) (Fig. 9(b), dotted line). Without ω_1, when the rf pulse area reaches 2π, all population should be returned to state

$|2\rangle$ so that transparency would be expected. However, the population accumulated in state $|3\rangle$ by the optical excitation at ω_1 produces gain.

In Fig. 10(a), we numerically demonstrated that rf-coupled optical gain is possible even without population inversion. These plots were generated by solving the three-level density matrix equations as a function of rf detuning for three different cases of optical homogeneous decay rates γ. We used parameters that were close to the experimental conditions. The rf pulse area was assumed to be 2π. Fig. 10(b) shows population difference ($\rho_{33} - \rho_{22}$) which is same for all three cases. Even though the ground state population is larger than that of the excited state at rf-photon resonance, the probe has gain if the rf power is strong enough ($\Omega_{rf} > \gamma$). Unfortunately, we have not experimentally seen this inversionless optical gain because of our rf power limitation.

5. Conclusion

In summary, we reviewed the first EIT observation in a persistent spectral hole-burning solid, Pr:YSO, and also reviewed some potential EIT applications that can benefit from this observation such as enhanced four-wave mixing, optical data storage, and lasers without inversion. The enhanced four-wave mixing signals also have potential applications to up-conversion lasers using solids. We also showed that spin coherences can be excited and rephased efficiently by using resonant Raman pulses. Achieving this high spin echo efficiency without the need for atomic state preparation, high power lasers, or long interaction times, is important for applications ranging from high resolution spectroscopy to high-density, high-speed optical memory. The observed temperature insensitive spin dephasing time demonstrates the potential of higher capacity optical data storage at temperatures higher than required by conventional photon echo memories. Although the observed rf-coupled optical gain was mostly from the population inversion, LWI should be possible when the rf Rabi frequency exceeds the optical decay rate. In our experiment, the rf Rabi frequency was limited by the rf power amplifier to be less than the laser jitter,

hence gain without population inversion was not observed. Nonetheless, these preliminary observations are important for future LWI experiments in solids.

Acknowledgment

This study was supported by Air Force Research Laboratory (grant F30602-96-2-0100) and US Air Force Office of Scientific Research (grant F49620-96-1-0395), and partially supported by National Science Foundation (grant ECS 9421304).

Captions of figures

FIG. 1. Energy-level diagram of Pr:YSO

FIG. 2. Experimental setup for EIT and nondegenerate four-wave mixing: AO, acousto-optic modulator; BS, beam splitter; C.R., chart recorder; M, mirror; OSC, oscilloscope; PD, photo-diode.

FIG. 3. Transmission versus probe (ω_1) detuning at 2K for a coupling (ω_2) intensity of (a) 9, (b) 28, (c) 90, and (d) 280 W/cm^2.

FIG. 4. EIT with repump (ω_R) field blue-detuned by (a) 300 and (b) 600 kHz.

FIG. 5. (a) EIT and (b) enhanced four-wave mixing at 6K.

FIG. 6. Resonant Raman interaction with a three-level system in (a) bare state basis and (b) coherent state basis. (c) Resonant Raman field excited spin coherence Re(ρ_{12}) as a function of the Raman pulse area: (solid), $\Gamma=\gamma=0$; (dotted) $\Gamma=\gamma=3\Omega$; (dashed) $\Gamma=\Omega/30$ and $\gamma=\Omega$.

FIG. 7 Resonant Raman pulse excited spin echo at 5 K. (a) Resonant Raman pulse sequence. (b) Observed echo signals. The power of ω_R, ω_1, ω_2, and ω_P are 9, 21, 1.5, and 2.8 mW, respectively. (c) Theoretical echo signal intensities for $\Gamma=\Omega/10$ and $\gamma=\Omega$.

FIG. 8. Two-bit optical data storage by frequency-selective time-domain stimulated spin echo based on EIT at 6 K: d, d', data; e, e',echoes. The powers (cw) of ω_R, ω_1, ω_2, and ω_P are 2, 10, 30, and 10 mW.

FIG. 9. Probe transmission versus time when rf pulse is applied: (a) experiment and (b) theory; γ_o=300 kHz, Ω_o=16 kHz, Ω_{rf}=28 kHz, and Δ^{rf}_{inh}=30 kHz. Solid curve, probe transmission; dashed curve, population difference.

FIG. 10. Theoretical optical gain without population inversion: (a) probe coherence Im(ρ_{23}) and (b) population difference ($\rho_{33}-\rho_{22}$) versus rf detuning: Ω_o=10, Ω_{rf}=179, Γ_o=6, Γ_{rf}=0, γ_{rf}=4, Δ^{rf}_{inh}=100 radians, and γ_o as shown.

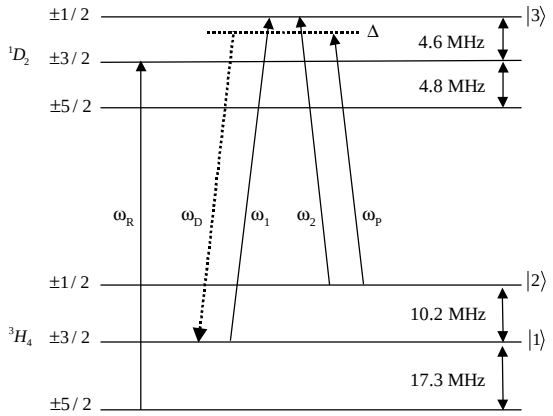
±1/2
|3⟩
Δ
4.6 MHz
$^1D_2$
±3/2
4.8 MHz
±5/2
ω_R
ω_D
ω_1
ω_2
ω_P
±1/2
|2⟩
10.2 MHz
$^3H_4$
±3/2
|1⟩
17.3 MHz
±5/2

Figure 1.

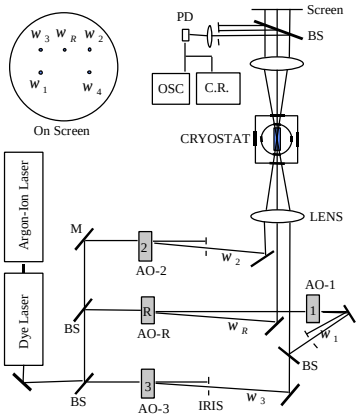
w 3
w R
w 2
w 1
w 4
On Screen
PD
Screen
BS
OSC
C.R.
CRYOSTAT
LENS
Argon-Ion Laser
Dye Laser
M
2
AO-2
w 2
AO-1
R
AO-R
w R
1
w 1
BS
BS
BS
3
AO-3
IRIS
w 3

Figure 2.

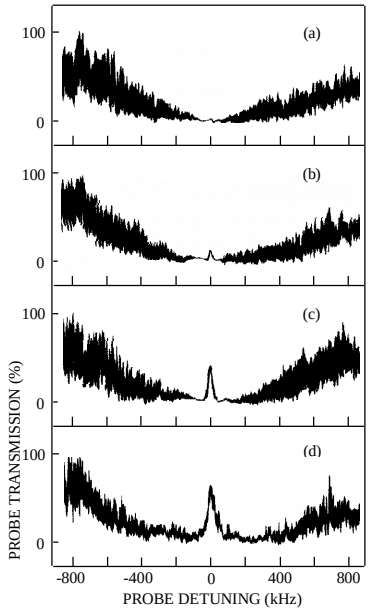
100
0
(a)
100
0
(b)
100
0
(c)
100
0
(d)
PROBE TRANSMISSION (%)
-800
-400
0
400
800
PROBE DETUNING (kHz)

Figure 3

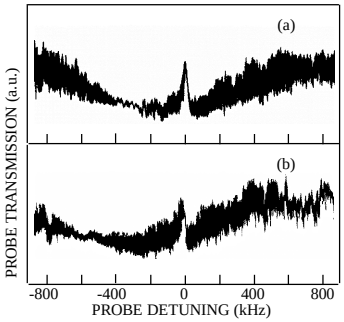
(a)
(b)
PROBE TRANSMISSION (a.u.)
-800
-400
0
400
800
PROBE DETUNING (kHz)

Figure 4

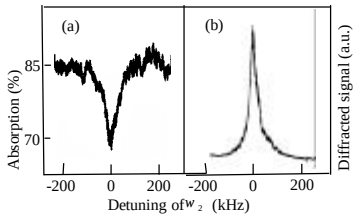

Figure 5.

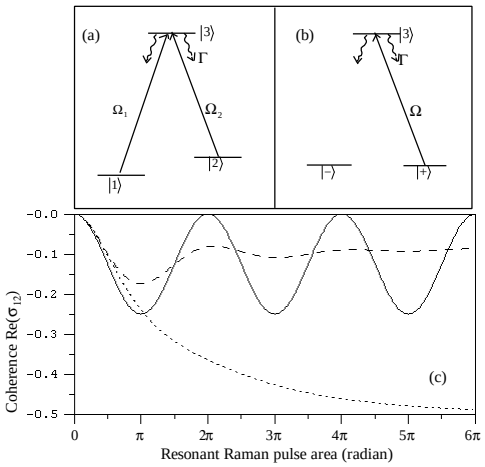

Figure 6.

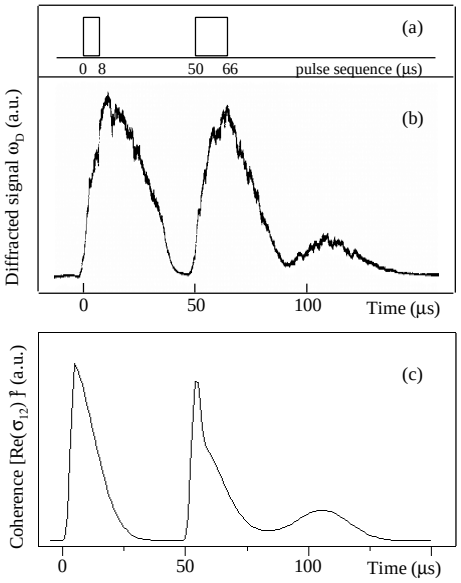
(a)
0 8
50 66
pulse sequence (μs)
(b)
Diffracted signal ω_D (a.u.)
0
50
100
Time (μs)
(c)
Coherence |Re(σ12)| f (a.u.)
0
50
100
Time (μs)

Figure 7.

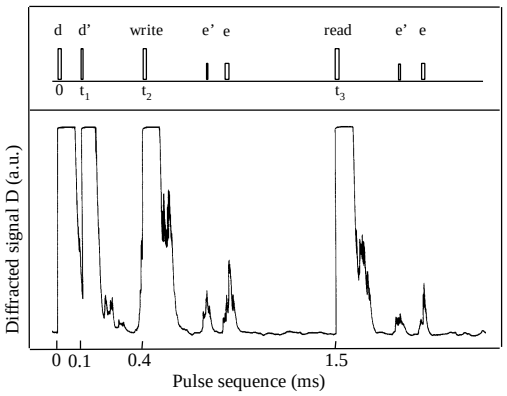
d
d'
write
e' e
read
e' e
0
t1
t2
t3
Diffracted signal D (a.u.)
0 0.1
0.4
1.5
Pulse sequence (ms)

Figure 8.

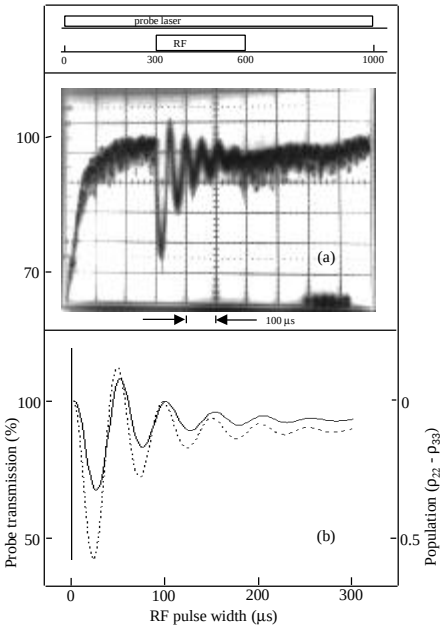
probe laser
RF
0
300
600
1000
100
70
(a)
100 µs
100
50
0
0.5
(b)
Probe transmission (%)
Population (ρ_{22} - ρ_{33})
0
100
200
300
RF pulse width (µs)

Figure 9.

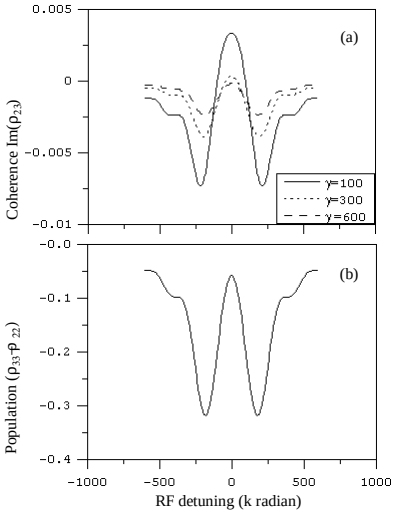
(a)
(b)
Coherence Im(ρ23)
Population (ρ33-ρ 22)
RF detuning (k radian)
γ=100
γ=300
γ=600
0.005
0
-0.005
-0.01
-0.0
-0.1
-0.2
-0.3
-0.4
-1000
-500
0
500
1000

Figure 10.

References

[1] G. Alzetta, A. Gozzini, L. Moi, and G. Orrilos, "An experimental method for the observation of rf transitions and laser beat resonances in oriented Na vapor," Nuovo Cimento B 36 (1976) 5.

[2] H. R. Gray, R. M. Whitley, and C. R. Stroud, Jr., "Coherent trapping of atomic populations," Opt. Lett. 3 (1978) 218.

[3] S. E. Harris, "Electromagnetically induced transparency," Phys. Today 50(7) (1997) 36, and references therein.

[4] M. P. Winters, J. L. Hall, and P. E. Toschek, "Correlated spontaneous emission in a Zeeman laser," Phys. Rev. Lett. 65 (1990) 3116.

[5] S. Harris, "Lasers without inversion; interference of lifetime-broadened resonances,"Phys. Rev. Lett. 62 (1989) 1033; A. S. Zibrov, M. D. Lukin, D. E. Nikonov, L. Hollberg, M. O. Scully, V. L. Velichansky, and H. G. Robinson, "Experimental demonstration of laser oscillation without population inversion via quantum interference in Rb," Phys. Rev. Lett. 75 (1995) 1499.

[6] S. E. Harris, J. E. Field, and A. Imamoglu, "Nonlinear optical processes using electromagnetically induced transparency," Phys. Rev. Lett. 64 (1990) 1107; M. Jain, H. Xia, G. Y. Yin, A. J. Merriam, and S. E. Harris, "Efficient nonlinear frequency conversion with maximal atomic coherence," Phys. Rev. Lett. 77 (1996) 4326.

[7] A. Kasapi, M. Jain, G. Y. Yin, and S. E. Harris, "Electromagnetically induced transparency: propagation dynamics," Phys. Rev. Lett. 74 (1995) 2447; J. H. Eberly, M. L. Pons, and H. R. Haq, "Dressed-field pulses in an absorbing medium," Phys. Rev. Lett. 72 (1994) 56.

[8] V. S. Sudarshanam, M. Cronin-Golomb, P. R. Hemmer, and M. S. Shahriar, "Turbulence-aberration correction with high-speed high-gain optical phase conjugation in sodium vapor," Opt. Lett. 22 (1997) 1141.

[9] M. D. Lukin, M. Fleischhauer, A. S. Zibrov, H. G. Robinson, V. L. Velichansky, L. Hollberg, and M. O. Scully, "Spectroscopy in dense coherent media: line narrowing and interference effects," Phys. Rev. Lett. **79**, 2959 (1997).

[10] M. O. Scully and M. Fleischhauer, "High-sensitivity magnetometer based on index-enhanced media," Phys. Rev. Lett. 69 (1992) 1360.

[11] P. R. Hemmer, K. Z. Cheng, J. Kierstead, M. S. Shahriar, M. K. Kim, "Time-domain optical data storage by use of Raman coherent population trapping," Opt. Lett. 19 (1994) 296.

[12] X. A. Shen. E. Chiang, and R. Kachru, "Time-domain holographic image storage," Opt. Lett. 19 (1994) 1246.

[13] B. S. Ham, M. S. Shahriar, M. K. Kim, and P. R. Hemmer, "Frequency-selective time-domain optical data storage by electromagnetically induced transparency in a rare-earth doped solid," Opt. Lett. 22 (1997) 1849.

[14] X. A. Shen and R. Kachru, "Optical header recognition by spectroholographic filtering," Opt. Lett. 20 (1995) 2508.

[15] Y. Zhang and R. Kachru, "Photon-echo novelty filters: a unique time-differential sensor of optical wave-front distortion caused by airborne turbulence," Appl. Opt. 37 (1998) 3246.

[16] B. S. Ham, P. R. Hemmer, and M. S. Shahriar, "Observation of laser-jitter-enhanced hyperfine spectroscopy and two-photon spectral hole burning," Opt. Commun. (submitted).

[17] T. Pellizzari, S. A. Gardiner, J. I. Cirac, and P. Zoller, "Decoherence, continuous observation, and quantum computing: a cavity QED model," Phys. Rev. Lett. 75 (1995) 3788.

[18] B. S. Ham, "Experimental study of lasing without population inversion in ruby," doctoral dissertation (Wayne State University, Detroit, MI 1995); Y. Zhao, C. Wu, B. S. Ham, M. K. Kim, and E. Awad, "Microwave induced transparency in ruby," Phys. Rev. Lett. 79 (1997) 641.

[19] B. S. Ham, P. R. Hemmer, and M. S. Shahriar, "Efficient electromagnetically induced transparency in a rare-earth doped crystal," Opt. Commun. 144 (1997) 227.

[20] B. S. Ham, M. S. Shahriar, and P. R. Hemmer, "Enhanced nondegenerate four-wave mixing owing to electromagnetically induced transparency in a spectral hole-burning crystal," Opt. Lett. 22 (1997) 1138.

[21] B. S. Ham, M. S. Shahriar, and P. R. Hemmer, "Radio-frequency-induced optical gain in Pr^{3+}:Y_2SiO_5," J. Opt. Soc. Am. B 15 (1998) 1541.

[22] K. Holliday, M. Croci, E. Vauthey, U. P. Wild, "Spectral hole burning and holography in an Y_2SiO_5:Pr^{3+} crystal," Phys. Rev. B 47 (1993) 14741.

[23] R. W. Equall, R. L. Cone, and R. M. Macfarlane, "Homogeneous broadening and hyperfine structure of optical transitions in Pr^{3+}:Y_2SiO_5," Phys. Rev. B 52 (1995) 3963.

[24] L. E. Eriction, "The nuclear quadrupole interaction in Pr^{3+}:LaF_3 – an optical-rf double resonance measurement of the ground electronic state," Opt. Commun. 21 (1977) 147.
[25] B. S. Ham, M. S. Shahriar, M. K. Kim, and P. R. Hemmer, "Spin coherence excitation and rephasing with optically shelved atoms," Phys. Rev. B 58 (1998) R11825.
[26] B. S. Ham, P. R. Hemmer, and M. S. Shahriar, "Enhancement of four-wave mixing and line narrowing by use of quantum coherence in an optically dense double-Λ solid," Opt. Lett. 24 (1999) No. 2. (In press).
[27] M. Kaivola, P. Thorsen, and O. Poulsen, "Dispersive line shapes and optical pumping in a three-level system," Phys. Rev. A 32 (1985) 207.
[28] Y. –Q. Li, S. -Z. Jin, and M. Xiao, "Observation of an electromagneticaly induced change of absorption in multilevel rubidium atoms," Phys. Rev. A 51 (1995) R1754.
[29] Y. Hukuda, K. Yamada, and T. Hashi, "Sublevel echoes induced by resonant light pulses: quantum beat echoes," Opt. Commun. 44 (1983) 297.
[30] E. C. Hoffmann, M. Hubrich, and A. Schweiger, "Primary nuclear spin echoes in EPR induced by microwave pulses," J. of Mag. Reson. A 117 (1995) 16.
[31] B. Lu, W. H. Burkett, and M. Xiao, "Nondegenerate four-wave mixing in a double-Λ system under the influence of coherent population trapping," Opt. Lett. 23 (1998) 804.
[32] S. Babin, U. Hinze, E. Tiemann, and B. Wellegehausen, "Continuous resonant four-wave mixing in double-Λ level configuration of Na_2," Opt. Lett. 21 (1996) 1186.